On the development of a dispersion-relation-preserving dual-compact upwind scheme for convection–diffusion equation

P.H. Chiu [a], Tony W.H. Sheu [a,b,c,*]

[a] Department of Engineering Science and Ocean Engineering, National Taiwan University, No. 1, Sec. 4, Roosevelt Road, Taipei, Taiwan, ROC
[b] Taida Institute of Mathematical Sciences (TIMS), National Taiwan University, Taipei, Taiwan, ROC
[c] Center of Quantum Science and Engineering (CQSE), National Taiwan University, Taipei, Taiwan, ROC

ARTICLE INFO

ABSTRACT

In this paper a dual-compact scheme, which accommodates a better dispersion relation for the convective terms shown in the transport equation, is proposed to enhance the convective stability of the convection–diffusion equation by virtue of the increased dispersive accuracy. The dispersion-relation-preserving compact scheme has been rigorously developed within the three-stencil point framework through the dispersion and dissipation analyses. To verify the proposed method, several problems that are amenable to the exact and benchmark solutions will be investigated. The results with good rates of convergence are demonstrated for all the investigated problems.

© 2009 Elsevier Inc. All rights reserved.

1. Introduction

Numerical simulation of convection–diffusion equation involves reducing the indispensable dispersion error, which is defined as the discrepancy between the effective and actual wave numbers. It is therefore important to apply a scheme with the ability to enhance convective stability when solving the practically and academically important convection-dominated convection–diffusion scalar transport equation and Navier–Stokes equations at high Reynolds numbers. To overcome the difficulty regarding the convective instability, many upwinding schemes have been proposed; see, e.g. [1–5]. Thanks to the underlying M-matrix theorem, the monotonic upwind schemes have been shown to be effective in enhancing convective stability [6,7]. Another theory that may also be adopted to enhance convective stability is to take the dispersive nature of the investigated first-order derivative term into consideration [8].

A scheme for approximating the convection terms can be rigorously said to preserve the dispersion relation if it accommodates the same dispersion relation as that of the original first-order derivative term [8]. This relation, which can be normally derived by performing the spatial Fourier transform on the first-order derivative term, characterizes the angular frequency relation with respect to the wavenumber of the spatial derivative term [9]. The main reason of developing the dispersion-relation-preserving (DRP) scheme is that some numerical features such as the dispersion, dissipation, group and phase velocities for each wave component supported by the first-order derivative term can be well modeled [10].

The idea of the combined compact difference (CCD) scheme, which was proposed by Chu and Fan [11], is to solve the first and second derivatives simultaneously. The resulting scheme becomes more compact and accurate than the normal difference schemes developed under the same number of stencil points. In addition, the dispersion error for this type of scheme is

* Corresponding author. Address: Department of Engineering Science and Ocean Engineering, National Taiwan University, No. 1, Sec. 4, Roosevelt Road, Taipei, Taiwan, ROC. Tel.: +886 2 33665746; fax: +886 2 23929885.
E-mail address: twhsheu@ntu.edu.tw (T.W.H. Sheu).

smaller. In the above light, we are motivated to couple the compact expressions for the first-order and second-order derivative terms. The underlying idea chosen to determine the relation between the two compact representations is to conduct the standard modified equation analysis, which involves truncated Taylor series, together with the Fourier transform analysis [12], which enables us to derive the same or almost the same dispersion relation as the original partial differential equation, during the approximation of convective and diffusive terms.

This paper is organized as follows. Section 2 presents the dual-compact scheme for the convection–diffusion equation within the three-point stencil. This is followed by the presentation of the compact scheme detailed in Section 3 for the second-order derivative term and in Section 4 for the dispersion-relation-preserving compact upwinding scheme for the first-order derivative term. Section 5 presents the simulated results to verify the proposed dual-compact method. In Section 7 we draw some concluding remarks based on the results presented in Section 6.

2. Dual-compact scheme

The scalar transport equation given below for a field variable ϕ will be considered:

$$a\frac{\partial \phi}{\partial x} + b\frac{\partial \phi}{\partial y} - k\left(\frac{\partial^2 \phi}{\partial x^2} + \frac{\partial^2 \phi}{\partial y^2}\right) = f \tag{1}$$

where k is the diffusion coefficient, and a and b are denoted as the constant velocities along the x- and y-direction, and f is the source term, respectively. Both of the first-order and second-order spatial derivative terms shown in Eq. (1) will be approximated at the uniform gird size $\Delta x = \Delta y = h$.

We assume that the first derivative term $\frac{\partial \phi}{\partial x}$ and the second derivative term $\frac{\partial^2 \phi}{\partial x^2}$, for example, in Eq. (1) are approximated respectively within the following three-point compact framework

$$a_1\frac{\partial \phi}{\partial x}\Big|_{i-1} + \frac{\partial \phi}{\partial x}\Big|_i = \frac{1}{h}(c_1\phi_{i-1} + c_2\phi_i + c_3\phi_{i+1}) - h\left(b_1\frac{\partial^2 \phi}{\partial x^2}\Big|_{i-1} + b_2\frac{\partial^2 \phi}{\partial x^2}\Big|_i + b_3\frac{\partial^2 \phi}{\partial x^2}\Big|_{i+1}\right) \tag{2}$$

$$\bar{b}_1\frac{\partial^2 \phi}{\partial x^2}\Big|_{i-1} + \frac{\partial^2 \phi}{\partial x^2}\Big|_i + \bar{b}_3\frac{\partial^2 \phi}{\partial x^2}\Big|_{i+1} = \frac{1}{h^2}(\bar{c}_1\phi_{i-1} + \bar{c}_2\phi_i + \bar{c}_3\phi_{i+1}) - \frac{1}{h}\left(\bar{a}_1\frac{\partial \phi}{\partial x}\Big|_{i-1} + \bar{a}_2\frac{\partial \phi}{\partial x}\Big|_i + \bar{a}_3\frac{\partial \phi}{\partial x}\Big|_{i+1}\right) \tag{3}$$

For terms $\frac{\partial \phi}{\partial y}$ and $\frac{\partial^2 \phi}{\partial y^2}$, they can be similarly expressed along the y-direction. Note that the compact schemes for $\frac{\partial \phi}{\partial x}\big|_i$ and $\frac{\partial^2 \phi}{\partial x^2}\big|_i$ are not independent of each other. They are rather strongly coupled through terms $\frac{\partial \phi}{\partial x}\big|_{i-1}, \frac{\partial \phi}{\partial x}\big|_i, \frac{\partial \phi}{\partial x}\big|_{i+1}, \frac{\partial^2 \phi}{\partial x^2}\big|_{i-1}, \frac{\partial^2 \phi}{\partial x^2}\big|_i, \frac{\partial^2 \phi}{\partial x^2}\big|_{i+1}, \phi_{i-1}, \phi_i$ and ϕ_{i+1}. For the sake of description, we consider the above equation only for the case involving the positive convective coefficient. As for the negative convective coefficient, the derivation can be done in the similar way.

3. Compact scheme for the second-order derivative term

Approximation of $\frac{\partial^2 \phi}{\partial x^2}$ can be normally made by applying the central schemes since the discretization error will be prevailingly dissipative. For this reason, the weighting coefficients shown in Eq. (3) will be determined solely by the modified equation analysis for rendering a higher spatial accuracy. Derivation of the coefficients $\bar{a}_1, \bar{a}_2, \bar{a}_3, \bar{b}_1, \bar{b}_3, \bar{c}_1, \bar{c}_2$ and $\bar{c}_3$ is as follows. We start by applying the Taylor series expansions for $\phi_{i\pm1}, \frac{\partial \phi}{\partial x}\big|_{i\pm1}$ and $\frac{\partial^2 \phi}{\partial x^2}\big|_{i\pm1}$ with respect to $\phi_i, \frac{\partial \phi}{\partial x}\big|_i$ and $\frac{\partial^2 \phi}{\partial x^2}\big|_i$ and, then, eliminating the leading error terms derived in the modified equation. This elimination of the leading error terms enables us to derive the following set of algebraic equations for Eq. (3)

$$\bar{c}_1 + \bar{c}_2 + \bar{c}_3 = 0 \tag{4}$$

$$-\bar{a}_1 - \bar{a}_2 - \bar{a}_3 - \bar{c}_1 + \bar{c}_3 = 0 \tag{5}$$

$$\bar{a}_1 - \bar{a}_3 - \bar{b}_1 + \frac{\bar{c}_1}{2} - \bar{b}_3 + \frac{\bar{c}_3}{2} = 1 \tag{6}$$

$$-\frac{\bar{a}_1}{2} - \frac{\bar{a}_3}{2} + \bar{b}_1 - \bar{b}_3 - \frac{\bar{c}_1}{6} + \frac{\bar{c}_3}{6} = 0 \tag{7}$$

$$\frac{\bar{a}_1}{6} - \frac{\bar{a}_3}{6} - \frac{\bar{b}_1}{2} + \frac{\bar{c}_1}{24} - \frac{\bar{b}_3}{2} + \frac{\bar{c}_3}{24} = 0 \tag{8}$$

$$-\frac{\bar{a}_1}{24} - \frac{\bar{a}_3}{24} + \frac{\bar{b}_1}{6} - \frac{\bar{b}_3}{6} - \frac{\bar{c}_1}{120} + \frac{\bar{c}_3}{120} = 0 \tag{9}$$

$$\frac{\bar{a}_1}{120} - \frac{\bar{a}_3}{120} - \frac{\bar{b}_1}{24} - \frac{\bar{b}_3}{24} + \frac{\bar{c}_1}{720} + \frac{\bar{c}_2}{720} = 0 \tag{10}$$

$$-\frac{\bar{a}_1}{720} - \frac{\bar{a}_3}{720} + \frac{\bar{b}_1}{120} - \frac{\bar{b}_3}{120} - \frac{\bar{c}_1}{5040} + \frac{\bar{c}_3}{5040} = 0 \tag{11}$$

By solving Eqs. (4)–(11), we can derive the coefficients for Eq. (3) as $\bar{a}_1 = -\frac{9}{8}, \bar{a}_2 = 0, \bar{a}_3 = \frac{9}{8}, \bar{b}_1 = -\frac{1}{8}, \bar{b}_3 = -\frac{1}{8}, \bar{c}_1 = 3, \bar{c}_2 = -6, \bar{c}_3 = 3$.

Note that the coefficients shown above in Eq. (3) are exactly the same as those given in Chu and Fan [11]. It is also remarked that by virtue of the following derived modified equation, the presently derived coefficients can render the approximation of $\frac{\partial^2 \phi}{\partial x^2}$ with the spatial accuracy order of sixth

$$\frac{\partial^2 \phi}{\partial x^2} = \frac{\partial^2 \phi}{\partial x^2}\bigg|_{exact} + \frac{h^6}{20160}\frac{\partial^8 \phi}{\partial x^8} + \frac{h^8}{604800}\frac{\partial^{10} \phi}{\partial x^{10}} + O(h^{12}) + \cdots$$

4. Dispersion-relation-preserving compact scheme for the first-order derivative term

The coefficients $a_1, b_1, b_2, b_3, c_1, c_2$ and c_3 are partly determined by applying the Taylor series expansions for $\phi_{i\pm1}, \frac{\partial \phi}{\partial x}\big|_{i-1}$ and $\frac{\partial^2 \phi}{\partial x^2}\big|_{i\pm1}$ with respect to $\phi_i, \frac{\partial \phi}{\partial x}\big|_i$ and $\frac{\partial^2 \phi}{\partial x^2}\big|_i$. By eliminating the leading error terms derived in the modified equation, the following set of algebraic equations for Eq. (2) can be derived as

$$c_1 + c_2 + c_3 = 0 \tag{12}$$
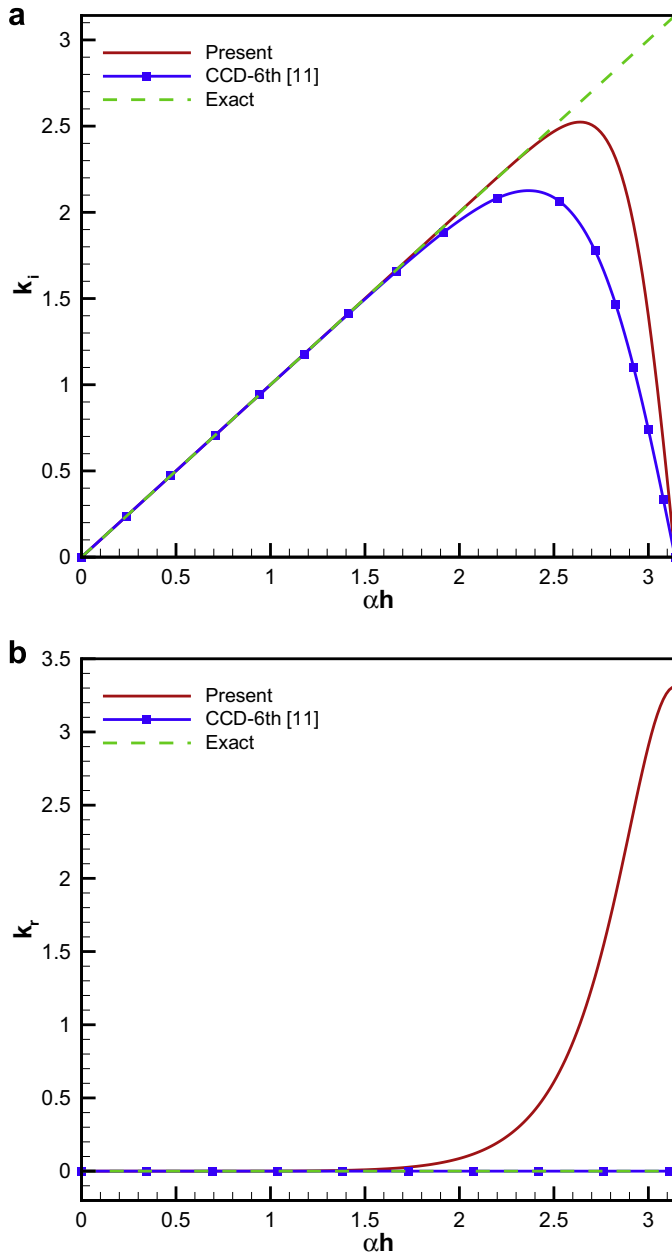$$-a_1 - c_1 + c_3 = 1 \tag{13}$$

Fig. 1. Comparison of k_r and k_i, which are plotted against αh, for the proposed dual-compact scheme and the CCD scheme of Chu and Fan [11]. (a) k_i and (b) k_r.

$$- a_1 + b_1 + b_2 + b_3 - \frac{c_1}{2} - \frac{c_3}{2} = 0 \tag{14}$$

$$\frac{a_1}{2} - b_1 + b_3 + \frac{c_1}{6} - \frac{c_3}{6} = 0 \tag{15}$$

$$-\frac{a_1}{6} + \frac{b_1}{2} + \frac{b_3}{2} - \frac{c_1}{24} - \frac{c_3}{24} = 0 \tag{16}$$

$$\frac{a_1}{24} - \frac{b_1}{6} + \frac{b_3}{6} + \frac{c_1}{120} - \frac{c_3}{120} = 0 \tag{17}$$

It is still short of one algebraic equation for us to uniquely determine all the seven introduced coefficients shown in Eq. (2).

For physically accurate predicting the first derivative term from Eq. (2), the dispersive nature embedded in $\frac{\partial \phi}{\partial x}$ must be retained as much as possible. The reason is that the dispersion relation governs the relation between the angular frequency and the wavenumber of the first-order dispersive term [8]. In other words, the solution can be accurately predicted provided that the dispersion relation is well preserved. Hence it is of primary importance to develop a scheme which accommodates the dispersion relation for the first-order derivative term.

To preserve the dispersion relation, the Fourier transform and its inverse for ϕ given below will be applied

$$\tilde{\phi}(\alpha) = \frac{1}{2\pi} \int_{-\infty}^{+\infty} \phi(x) \ \exp(-\mathbf{i}\,\alpha x) \ dx, \tag{18}$$

$$\phi(x) = \int_{-\infty}^{+\infty} \tilde{\phi}(\alpha) \ \exp(\mathbf{i}\,\alpha x) \ d\alpha. \tag{19}$$
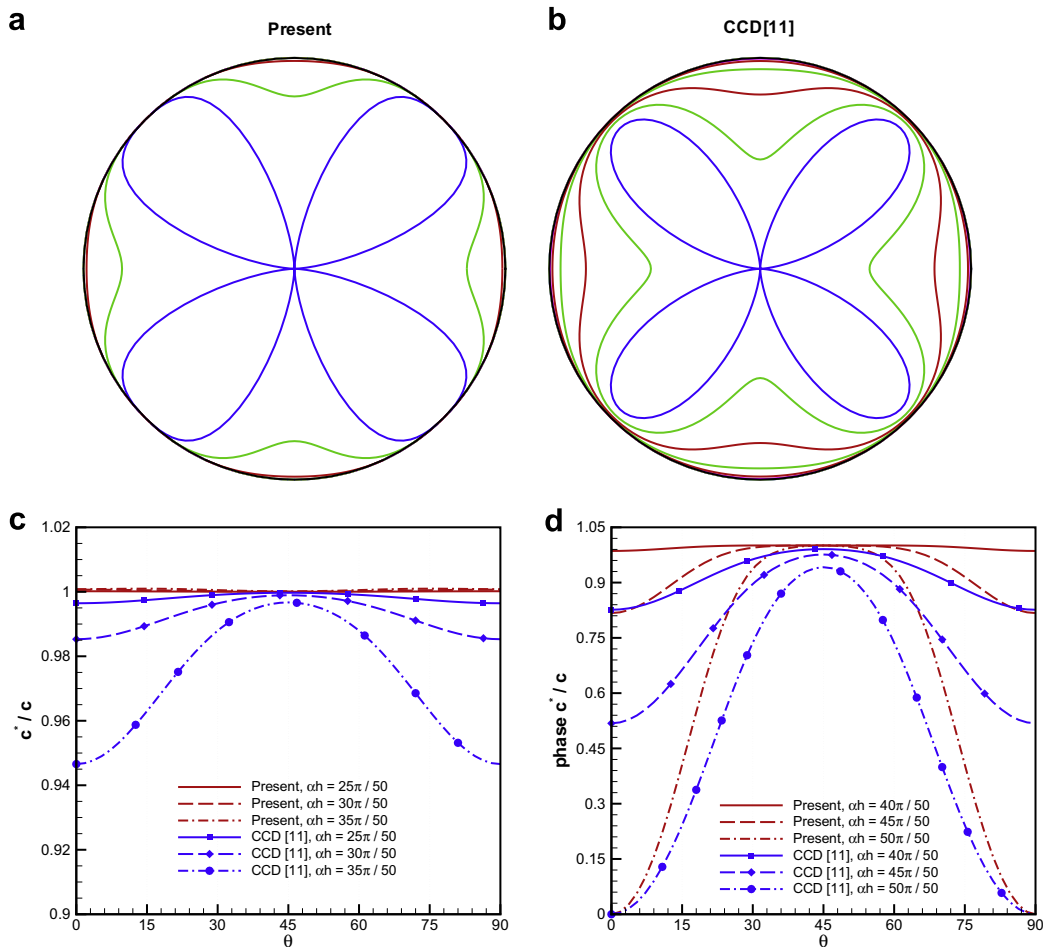

Fig. 2. Comparison of the predicted phase speed anisotropy, which is plotted against θ, for the proposed dual-compact scheme and the CCD scheme of Chu and Fan [11]. (a) Present scheme; (b) CCD scheme [11]; (c–d) Comparison of the present and CCD schemes in terms of c^*/c, which represents the ratio of the phase speed with respect to the analytic propagation speed, against the angle θ at different values of the modified wavenumber αh.

Table 1
The computed L_2-error norms and the corresponding spatial rates of convergence (s.r.c.) for the calculations carried out at five chosen meshes using the proposed dual-compact scheme and CCD scheme [11] for $Re = 1$.

Meshes	Present		CCD [11]	
	L_2-error norms	s.r.c.	L_2-error norms	s.r.c.
10×10	1.081E−6	–	1.050E−6	–
15×15	1.629E−7	4.669	1.589E−7	4.658
20×20	4.151E−8	4.751	4.054E−8	4.749
25×25	1.411E−8	4.836	1.378E−8	4.835
30×30	5.950E−9	4.736	5.823E−9	4.725

Table 2
The computed L_2-error norms and the corresponding spatial rates of convergence (s.r.c.) for the calculations carried out at five chosen meshes using the proposed dual-compact scheme and CCD scheme [11] for $Re = 10$.

Meshes	Present		CCD [11]	
	L_2-error norms	s.r.c.	L_2-error norms	s.r.c.
10×10	1.392E−6	–	1.294E−6	–
15×15	2.045E−7	4.730	1.924E−7	4.700
20×20	5.010E−8	4.889	4.736E−8	4.873
25×25	1.567E−8	5.208	1.486E−8	5.194
30×30	8.054E−9	3.650	7.920E−9	3.451

Table 3
The computed L_2-error norms and the corresponding spatial rates of convergence (s.r.c.) for the calculations carried out at five chosen meshes using the proposed dual-compact scheme and CCD scheme [11] for $Re = 100$.

Meshes	Present		CCD [11]	
	L_2-error norms	s.r.c.	L_2-error norms	s.r.c.
10×10	3.276E−6	–	2.999E−6	–
15×15	4.803E−7	4.734	3.953E−7	4.998
20×20	1.171E−7	4.906	9.707E−7	4.881
25×25	3.823E−8	5.016	3.194E−8	4.980
30×30	1.511E−8	5.090	1.273E−8	5.044

Table 4
The computed L_2-error norms and the corresponding spatial rates of convergence (s.r.c.) for the calculations carried out at five chosen meshes using the proposed dual-compact scheme for $Re = 10,000$ and $100,000$.

Meshes	$Re = 10,000$		$Re = 100,000$	
	L_2-error norms	s.r.c.	L_2-error norms	s.r.c.
10×10	4.341E−6	–	4.345E−6	–
15×15	6.772E−7	4.582	6.800E−7	4.580
20×20	1.773E−7	4.658	1.782E−7	4.653
25×25	6.161E−8	4.737	6.203E−8	4.730
30×30	2.574E−8	4.786	2.595E−8	4.778

Table 5
The computed L_2-error norms and the corresponding spatial rates of convergence for the calculations carried out at five chosen meshes using the proposed dual-compact scheme.

Mesh	L_2-error norm	Spatial rate of convergence
10×10	4.341E−6	–
15×15	6.772E−7	4.582
20×20	1.773E−7	4.658
25×25	6.161E−8	4.737
30×30	2.574E−8	4.786

Note that the notation **i** shown above is equal to $\sqrt{-1}$. Development of the dispersion-relation-preserving scheme is followed by performing Fourier transform on each term shown in Eqs. (2) and (3). The expressions of the actual wavenumber α for these two equations can be therefore derived as

$$\mathbf{i}\alpha h(a_1 \exp(-\mathbf{i}\alpha h) + 1) \simeq c_1 \exp(-\mathbf{i}\alpha h) + c_2 + c_3 \exp(\mathbf{i}\alpha h) - (\mathbf{i}\alpha h)^2 (b_1 \exp(-\mathbf{i}\alpha h) + b_2 + b_3 \exp(\mathbf{i}\alpha h)) \tag{20}$$

$$(\mathbf{i}\alpha h)^2 \left(-\frac{1}{8} \exp(-\mathbf{i}\alpha h) + 1 - \frac{1}{8} \exp(\mathbf{i}\alpha h) \right) \simeq 3 \exp(-\mathbf{i}\alpha h) - 6 + 3 \exp(\mathbf{i}\alpha h) - \mathbf{i}\alpha h \left(-\frac{8}{9} \exp(-\mathbf{i}\alpha h) + \frac{8}{9} \exp(\mathbf{i}\alpha h) \right) \tag{21}$$
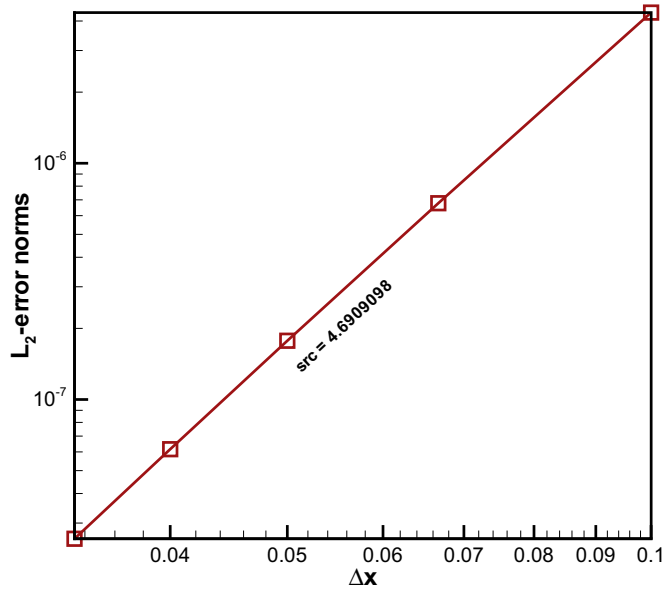

Fig. 3. The predicted spatial rate of convergence (src) based on the predicted L_2-error norms for the test problem given in Section 5.

Table 6
The computed CPU times for the calculations carried out at five chosen meshes using the proposed dual-compact scheme and the CCD scheme [11] for the case investigated at $Re = 100$.

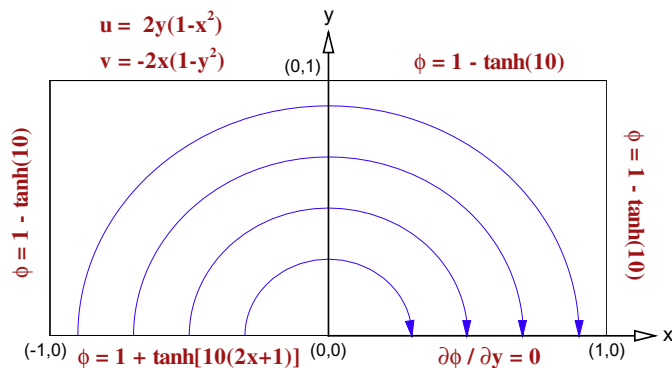| Meshes	Present	CCD [11]
10×10	0.262	0.251
15×15	0.492	0.468
20×20	1.495	1.421
25×25	2.212	2.078
30×30	5.937	5.703

Fig. 4. Schematic of the specified boundary conditions and the specified velocity vectors for the Smith–Hutton problem considered in Section 6.1.

In an approximation sense, the effective wavenumbers α' and α'' are derived to have the same expressions as those shown in the right-hand sides of Eqs. (20) and (21) [8]. For this reason, it is rational for us to express α' and α'' as follows:

$$\mathbf{i}\alpha'h(a_1 \exp(-\mathbf{i}\alpha h) + 1) = c_1 \exp(-\mathbf{i}\alpha h) + c_2 + c_3 \exp(\mathbf{i}\alpha h) - (\mathbf{i}\alpha''h)^2(b_1 \exp(-\mathbf{i}\alpha h) + b_2 + b_3 \exp(\mathbf{i}\alpha h)) \tag{22}$$

$$\mathbf{i}\alpha'h\left(-\frac{8}{9}\exp(-\mathbf{i}\alpha h) + \frac{8}{9}\exp(\mathbf{i}\alpha h)\right) = 3\exp(-\mathbf{i}\alpha h) - 6 + 3\exp(\mathbf{i}\alpha h) - (\mathbf{i}\alpha''h)^2\left(-\frac{1}{8}\exp(-\mathbf{i}\alpha h) + 1 - \frac{1}{8}\exp(\mathbf{i}\alpha h)\right) \tag{23}$$
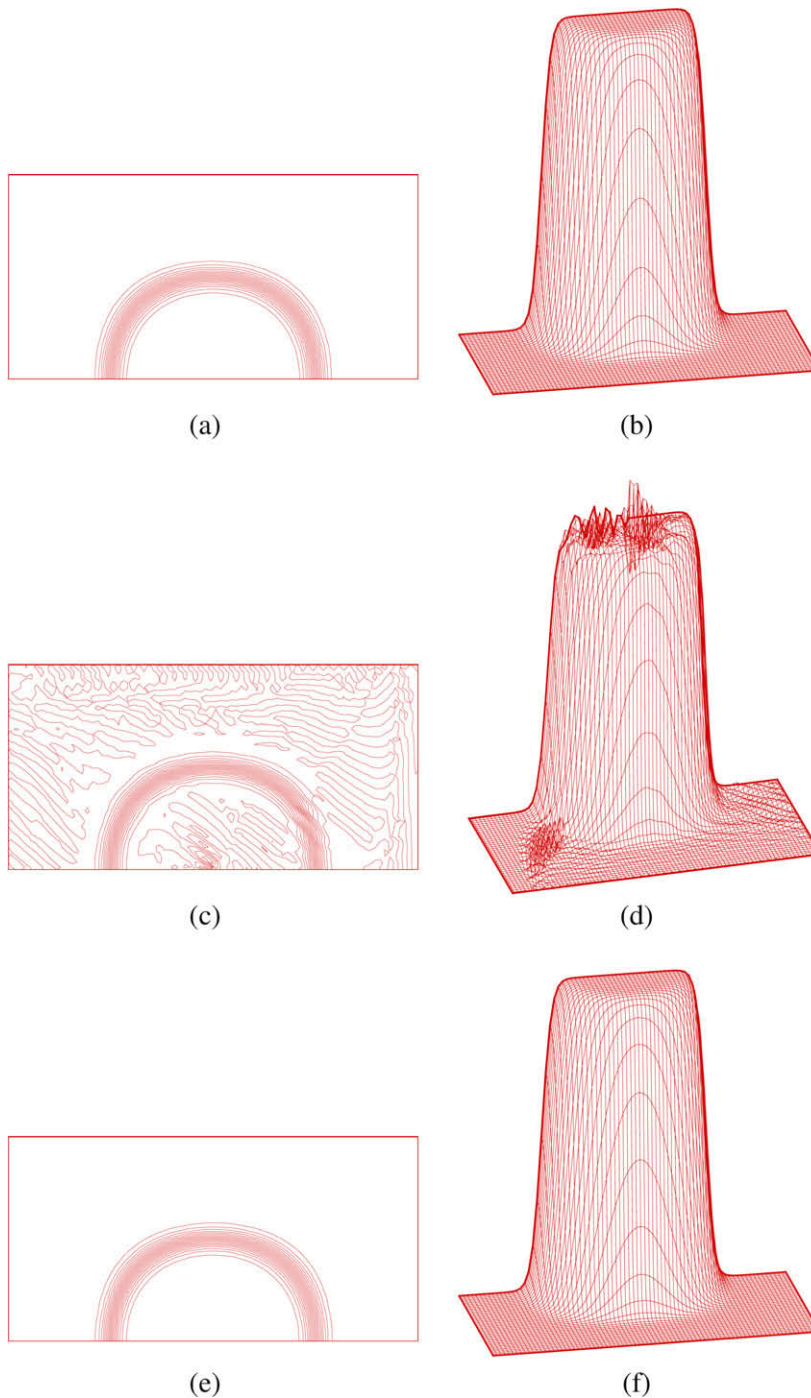

Fig. 5. The predicted two- and three-dimensional contours of ϕ for the problem considered in Section 6.1. (a)–(b) Present; (c)–(d) CCD [11]; (e)–(f) CCD [11] with damping. Note that the artificial viscosity k' shown in the numerically added damping term $k'\nabla^2\phi$ of Eq. (1) is 1/10,000.

By solving Eqs. (22) and (23), the following expressions for α' and α'' can be derived as

$$\alpha'h = -\mathbf{i}(24b_1\exp(-2\mathbf{i}\alpha h) + c_1\exp(-2\mathbf{i}\alpha h) + c_3 + c1 + 24b_1 + c_2\exp(-\mathbf{i}\alpha h) + 24b_2\exp(-\mathbf{i}\alpha h)$$

$$+ 24b_3 - 48b_1\exp(-\mathbf{i}\alpha h) - 8c_1\exp(-\mathbf{i}\alpha h) - 48b_3\exp(\mathbf{i}\alpha h) + 24b_2\exp(\mathbf{i}\alpha h) + 24b_3\exp(2\mathbf{i}\alpha h) - 48b_2$$

$$+ c_2\exp(\mathbf{i}\alpha h) + c_3\exp(2\mathbf{i}\alpha h) - 8c_3\exp(\mathbf{i}\alpha h) - 8c_2)/(-8 + \exp(\mathbf{i}\alpha h) - 8a_1\exp(-\mathbf{i}\alpha h) + a_1\exp(-2\mathbf{i}\alpha h)$$

$$- 9b_1\exp(-2\mathbf{i}\alpha h) - 9b_2\exp(-\mathbf{i}\alpha h) + 9b_2\exp(\mathbf{i}\alpha h) + 9b_3\exp(2\mathbf{i}\alpha h) + a_1 + 9b_1 - 9b_3 + \exp(\mathbf{i}\alpha h)) \tag{24}$$

$$\alpha''h = \sqrt{-\frac{3\exp(-\mathbf{i}\alpha h) - 6 + 3\exp(\mathbf{i}\alpha h) - \mathbf{i}\alpha'h\left(-\frac{8}{9}\exp(-\mathbf{i}\alpha h) + \frac{8}{9}\exp(\mathbf{i}\alpha h)\right)}{-\frac{1}{8}\exp(-\mathbf{i}\alpha h) + 1 - \frac{1}{8}\exp(\mathbf{i}\alpha h)}} \tag{25}$$

For the sake of acquiring a better dispersive accuracy for α', it is demanded that $\alpha h \approx \Re[\alpha'h]$, where $\Re[\alpha'h]$ denotes the real part of $\alpha'h$. This implies that $E(\alpha)$ defined below should be a very small and positive value

$$E(\alpha) = \int_{-\frac{\pi}{2}}^{\frac{\pi}{2}}[W(\alpha h - \Re[\alpha'h])]^2 d(\alpha h) = \int_{-\frac{\pi}{2}}^{\frac{\pi}{2}}[W(\gamma - \Re[\gamma'])]^2 d\gamma \tag{26}$$

where $\gamma = \alpha h$ and $\gamma' = \alpha'h$. Note that Eq. (26) can be analytically integrable provided that the weighting function W shown above is chosen as
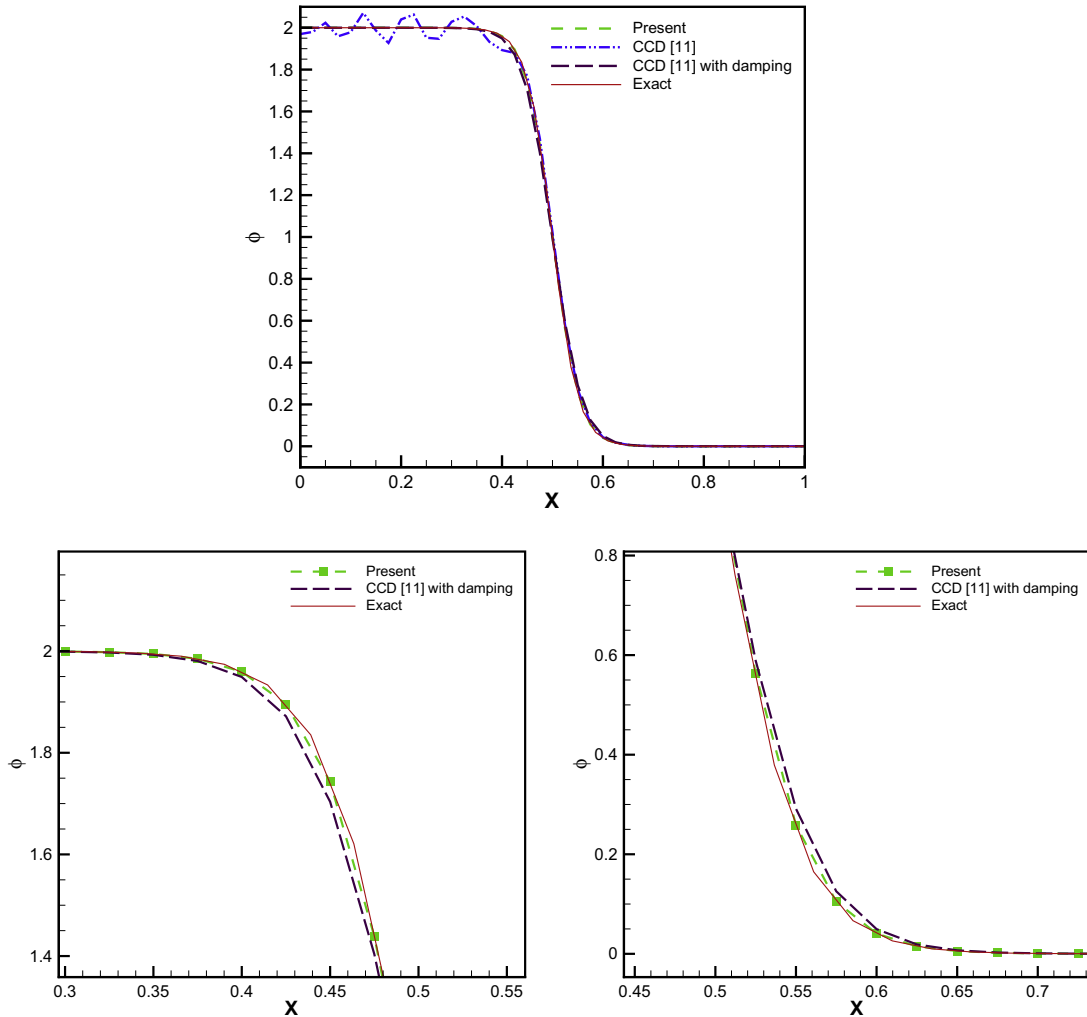

Fig. 6. Comparison of the predicted solution at $\Delta x = 1/40$ and the exact solution for ϕ plotted along the line given by $(0 \leqslant x \leqslant 1, y = 0)$ for the problem considered in Section 6.1.

$$W = -16 + 72b_3 + 72b_1 - 81b_1^2 - 81b_3^2 - 81b_2^2 - 162b_2b_3cos(\gamma) - 144a_1b_3cos(\gamma) - 162b_1b_2cos(\gamma) - a_1^2cos(\gamma)^2$$
$$+ 8a_1^2cos(\gamma) - 18b_3cos(\gamma)^3 + 18b_1cos(\gamma)^3 + 81b_2^2cos(\gamma)^2 + 162b_1b_3 - 72b_1cos(\gamma)^2 + 81b_3^2cos(\gamma)^2$$
$$+ 81b_1^2cos(\gamma)^2 - 72a_1b_2 - 18b_1cos(\gamma) + 16a_1cos(\gamma)^2 - 2a_1cos(\gamma)^3 + 72b_3cos(\gamma)^2 + 18b_3cos(\gamma) - 32a_1cos(\gamma)$$
$$- 36a_1b_3cos(\gamma)^4 - 18a_1b_2cos(\gamma)^3 + 162b_2b_3cos(\gamma)^3 + 162b_1b_2cos(\gamma)^3 + 324b_1b_3cos(\gamma)^4 + 72a_1b_2cos(\gamma)^2$$
$$+ 144a_1b_3cos(\gamma)^3 - 486b_1b_3cos(\gamma)^2 + 36a_1b_3cos(\gamma)^2 + 18a_1b_2cos(\gamma) + 8cos(\gamma) - 16a_1^2 - cos(\gamma)^2 \quad (27)$$

Note that W is the denominator of $(\gamma - \Re[\gamma'])$. It is also worth pointing out that the integration interval shown in Eq. (26) is sufficient to cover a complete period of the sine (or cosine) wave. To make E defined in Eq. (26) to be positive and minimum, the following extreme condition is enforced

$$\frac{\partial E}{\partial c_3} = 0 \quad (28)$$

The above equation, which is enforced to preserve the dispersion relation, will be used together with another six previously derived algebraic equations by way of the modified equation analysis to acquire a higher dissipation accuracy as well as a dispersion accuracy. The resulting seven introduced unknowns given below can be uniquely determined as

$$a_1 = 0.875 \quad (29)$$
$$b_1 = 0.12512823415990895606 \quad (30)$$
$$b_2 = -0.24871765840091043936 \quad (31)$$
$$b_3 = 0.00012823415990895606366 \quad (32)$$
$$c_1 = -1.9359611900810925272 \quad (33)$$
$$c_2 = 1.9969223801621850545 \quad (34)$$
$$c_3 = -0.060961190081092527237 \quad (35)$$

We remark here that the above upwinding scheme developed for $\frac{\partial \phi}{\partial x}$ can be easily shown to have the spatial accuracy order of fifth from the following modified equation

$$\frac{\partial \phi}{\partial x} = \frac{\partial \phi}{\partial x}\bigg|_{exact} - 0.00070085615243989922475h^5 \frac{\partial^6 \phi}{\partial x^6} + 0.0001984126984126984127h^6 \frac{\partial^7 \phi}{\partial x^7}$$
$$- 0.0000498830507458330390h^7 \frac{\partial^8 \phi}{\partial x^8} + O(h^8) + \cdots \quad (36)$$

Fundamental analysis of the present DRP scheme starts from defining the coefficients k_i and k_r for the respective dispersion and dissipation errors
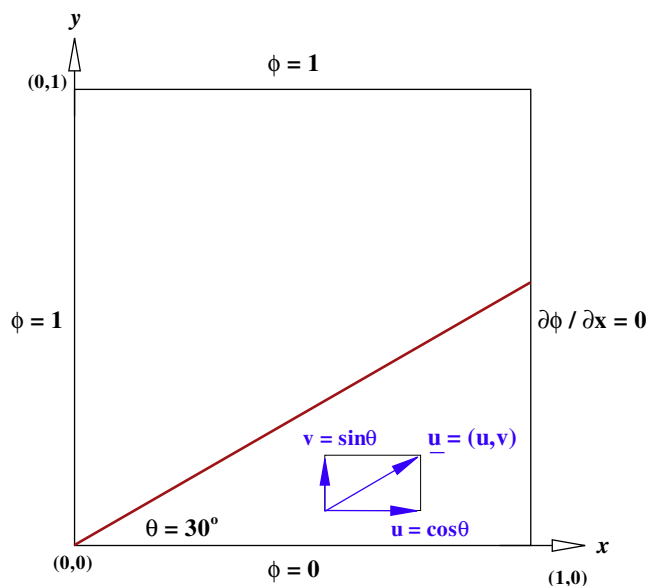

Fig. 7. Schematic of the convection–diffusion problem considered in Section 6.2.

$$k_i = \Re[\gamma'] \tag{37}$$
$$k_r = \Im[\gamma'] \tag{38}$$

In the above, $\Re[\gamma']$ denotes the real part of $\gamma' (\equiv \alpha' h)$ and $\Im[\gamma']$ stands for the imaginary part of γ' for the proposed scheme. In Fig. 1, the predicted values of k_i and k_r are plotted against the modified wavenumber αh for the present dual-compact upwinding scheme. One can easily see that the dispersion nature of the proposed scheme is better than the CCD scheme of Chu and Fan [11]. As for the k_r value derived from the current upwinded dual-compact scheme, it is less accurate than that derived from the non-dissipated central-type CCD scheme of Chu and Fan [11] due to the implicitly added artificial viscosity to the proposed scheme for the sake of enhanced stability.

We also plot in Fig. 2 the phase speed anisotropy [11,13], which is given below, for the present and CCD schemes

$$c^*/c(\gamma, \theta) = \frac{\cos(\theta)\Re[\gamma'(\gamma\cos(\theta))]\sin(\theta)\Re[\gamma'(\gamma\sin(\theta))]}{\gamma} \tag{39}$$

where θ is the angle between the propagation direction and the x axis. From Fig. 2, one can clearly see that the phase speed anisotropy for the proposed scheme is much accurate than the CCD scheme of Chu and Fan [11], in particular, at the angle of $\theta = 45°$.

5. Verification study

The following transport equation for ϕ will be solved in a square domain for the sake of analytically verifying the proposed dual-compact scheme:
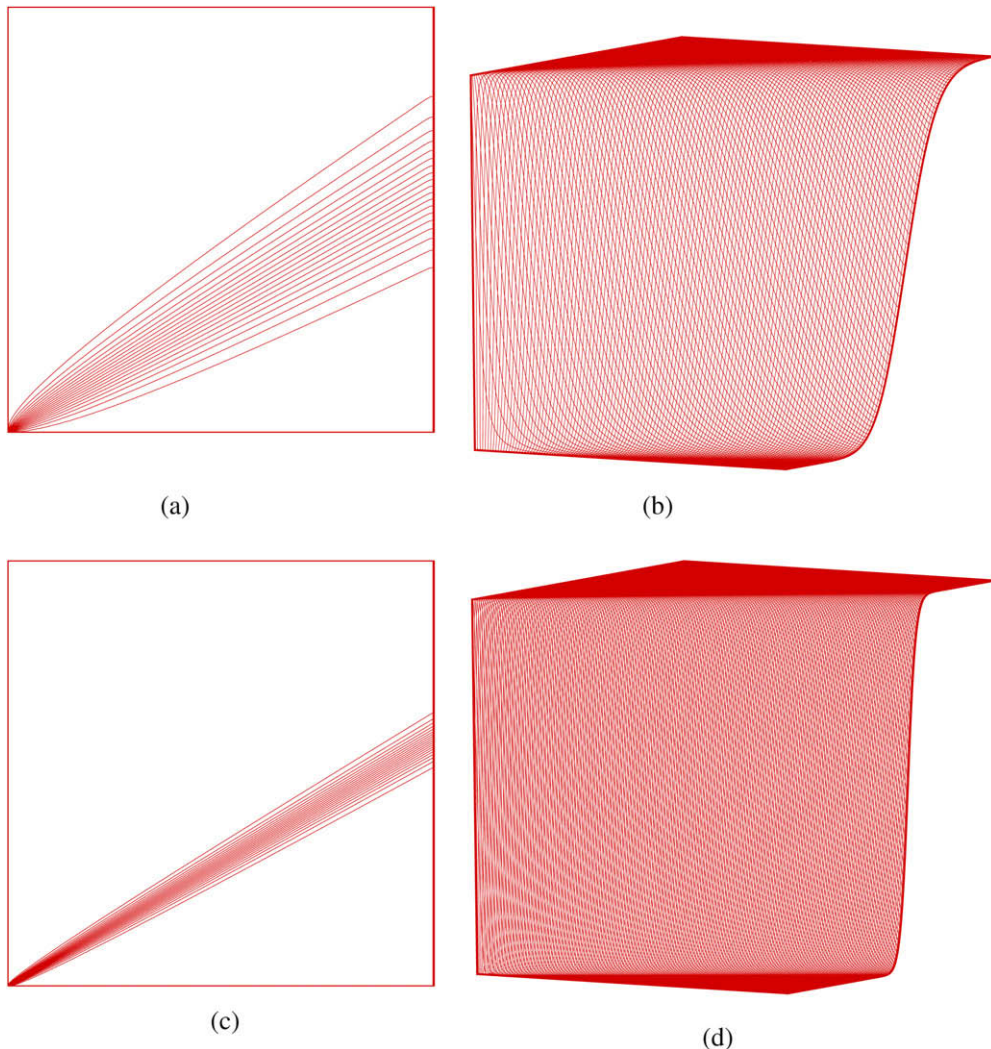

(a)   (b)

(c)   (d)

Fig. 8. The predicted two- and three-dimensional contours of ϕ for the problem considered in Section 6.2. (a)–(b) $Re = 100$; (c)–(d) $Re = 1000$.
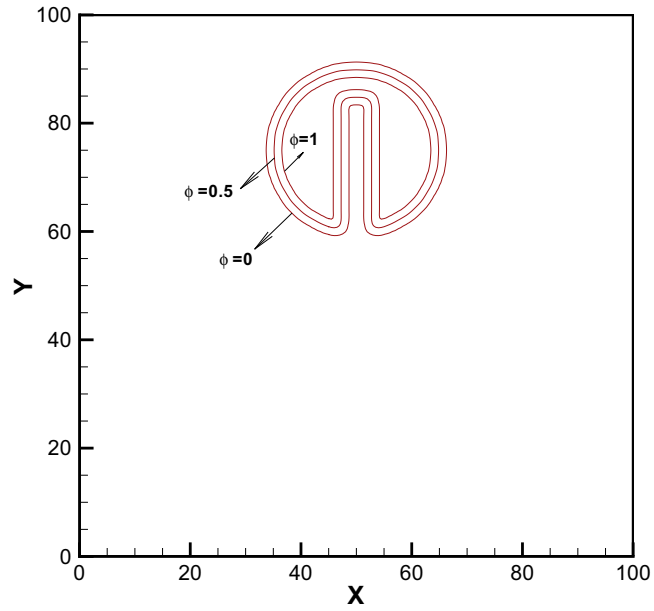
Fig. 9. Schematic of the initial ϕ contours for the Zalesak problem considered in Section 6.3.
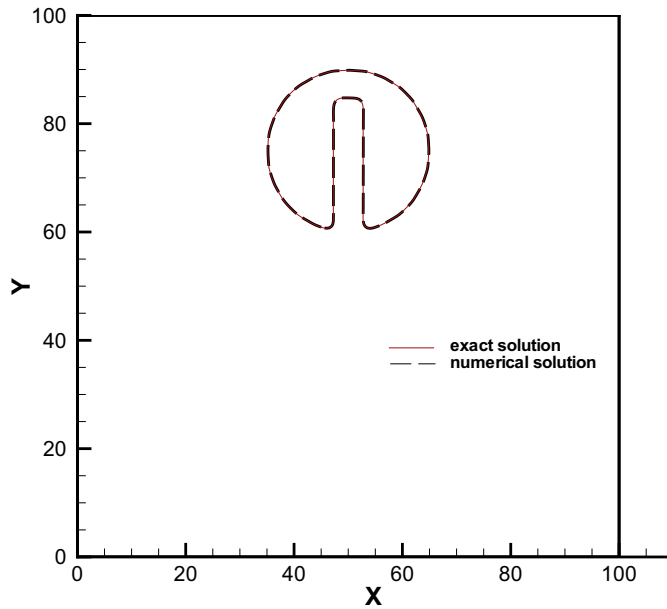

Fig. 10. The exact (solid line) and predicted (dashed line) contours for $\phi = 0.5$ at $t = 3140$ at the time after rotating the initially prescribed profile by five revolutions for the problem considered in Section 6.3.

$$u\frac{\partial \phi}{\partial x} + v\frac{\partial \phi}{\partial y} = \frac{1}{Re}\left(\frac{\partial^2 \phi}{\partial x^2} + \frac{\partial^2 \phi}{\partial y^2}\right) + S \tag{40}$$

In the above, Re and S are denoted as the Reynolds number and the source term per unit volume, respectively. The solution ϕ, subject to the following divergence-free velocity field [14], will be sought in $0 \leqslant x, y \leqslant 1$

$$u = \frac{-2(1+y)}{(1+x)^2 + (1+y)^2} \tag{41}$$

$$v = \frac{2(1+x)}{(1+x)^2 + (1+y)^2} \tag{42}$$

The analytic solution for ϕ has the same form as u given in (41) provided that the source term is chosen as $S = -\frac{\partial p}{\partial x}$, where

$$p = -\frac{2}{(1+x)^2 + (1+y)^2} \tag{43}$$

As usual, the currently proposed dual-compact scheme will be assessed through the nodal errors obtained in various meshes for the cases carried out at $Re = 1, 10, 100, 10000$ and $100,000$. At the boundary points, we apply the fourth-order accurate scheme, which is the same as the one employed in [11]. From Tables 1–4, good agreement with the exact solutions and the good spatial rates of convergence are based on the L_2-error norms computed at $10 \times 10, 15 \times 15, 20 \times 20, 25 \times 25, 30 \times 30$ nodal points. We also show the result in Table 5 and Fig. 3 for $Re = 10,000$. As can be seen from these predicted L_2-error norms, the dual-compact scheme is applicable to solve the two dimensional transport equation at high as well as low Reynolds numbers. We also assess the computational efficiency in terms of the CPU times for the implicit central CCD scheme and the current upwinded dual-compact scheme. In this comparison study, the twin-tridiagonal algebraic equation
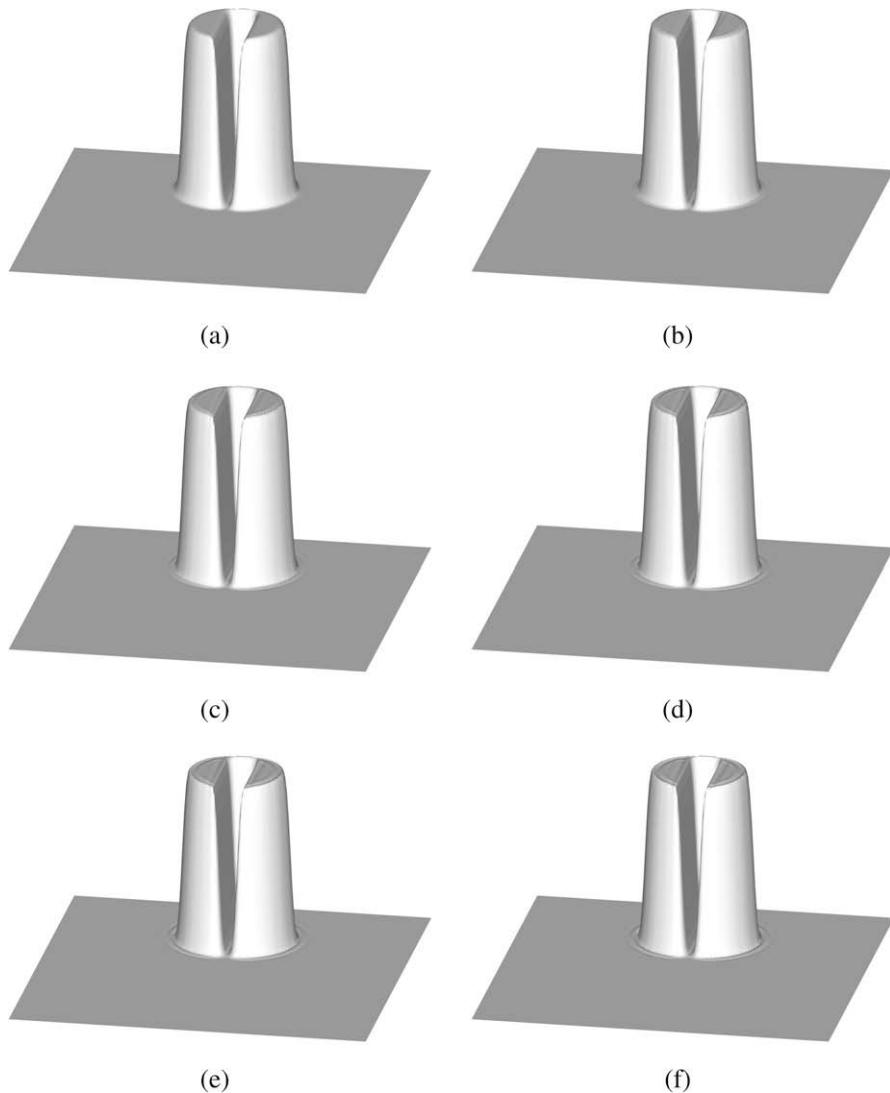

Fig. 11. The initial and the predicted three-dimensional contours of ϕ at different revolutions for the problem considered in Section 6.3. (a) Initial; (b) after one revolution; (c) after two revolutions; (d) after three revolutions; (e) after four revolutions; (f) after five revolutions.

will be solved by the computationally effective solver given in [11] at $Re = 100$. As can be clearly seen from Table 6 that the difference in the computational times is negligibly small.

6. Numerical studies

6.1. Convection–diffusion problem of Smith and Hutton

The problem of Smith and Hutton [15] will be investigated at $u = 2y(1 - x^2)$, $v = -2x(1 - y^2)$ and $S = 0$ shown in Eq. (40). Along the inlet schematic in Fig. 4, ϕ is prescribed by the distribution of $\phi(-1 \leqslant x \leqslant 0, y = 0) = 1 + \tanh[(2x + 1) \times 10]$. Along the lines $x = -1, y = 1$ and $x = 1$, ϕ is prescribed as $1 - \tanh(10)$ while along the outlet $(0 \leqslant x \leqslant 1, y = 0)$ a zero gradient condition is specified for ϕ. For the case investigated at $Re = \infty$ (or $k = 0$), the results calculated at $\Delta x = \Delta y = \frac{1}{40}$ are plotted in Fig. 5. The predicted oscillatory solution from the CCD scheme of Chu and Fan [11] is under our expectation since this central-type compact scheme suffers the problem of instability for the convection-dominated problems [16]. In order to suppress the instability, one can include the damping term $k' \nabla^2 \phi$ to the right-hand side of Eq. (40). It can be seen from Fig. 5 that the CCD scheme [11] with $k' = 1/10,000$ can resolve also the oscillations but is accompanied with a larger smearing of the solution in comparison with the current dual-compact solution ϕ plotted along the line $0 \leqslant x \leqslant 1, y = 0$. It can be seen from Fig. 6 that the predicted solutions from the proposed method are drastically accurate than the solutions computed from the CCD scheme [11]. The efficacy of the proposed dual-compact scheme is therefore revealed for the problem involving an interior sharp layer.

6.2. Skew convection–diffusion problem

In Fig. 7, a unit-square cavity is divided into two subdomains by the straight line, which passes through (0,0), with the slope of $\tan^{-1}(v/u)$, where u and v are shown in Eq. (40). We consider in this study the unit velocity vector (u, v), which is parallel to the dividing line, in 121×121 (for $Re = 100$) and 257×257 (for $Re = 1000$) uniformly discretized mesh systems for the problem with $S = 0$. Subject to the boundary conditions for the working variable ϕ, one can clearly see a shear layer with the width of $O(\sqrt{Re})$ in Fig. 8 in the vicinity of the dividing line. No oscillatory solution is found to occur both in regions near and apart from the dividing line for the cases with $Re = 100$ and 1000.

6.3. Transport of a sharp slot profile in a variable velocity flow field

To verify the proposed DRP advection scheme, the problem of Zalesak [17] will be considered. The sharp profile of the notched disc with the slot width of 15 is made to rotate about the point (50,75) in an inviscid flow given by
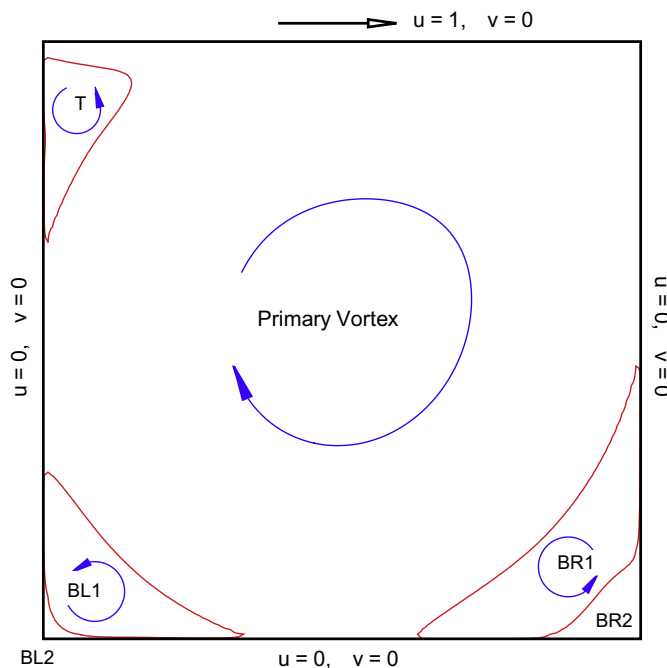

Fig. 12. Schematic of the eddy centers possibly formed in the lid-driven cavity.

$(u, v) = ((\pi/314)(50 - y), (\pi/314)(x - 50))$, which corresponds to the stream function given by $\psi = \frac{x}{2} + \frac{y}{2} - \frac{x^2}{200} - \frac{y^2}{200}$. At $t = 0$, function ϕ needs to be slightly smeared to avoid discontinuity in the initially prescribed profile. For the sake of smoothly preserving the sharp front, ϕ approximated in a way given below can retain its interface, schematic in Fig. 9, as steep as possible

$$\phi = \begin{cases} 0; & \text{if } |\underline{x}| > 3\delta \\ \frac{1}{(1+e^{\underline{x}/\delta})}; & \text{if } -3\delta \leqslant |\underline{x}| \leqslant 3\delta \\ 1; & \text{if } |\underline{x}| < -3\delta \end{cases} \tag{44}$$
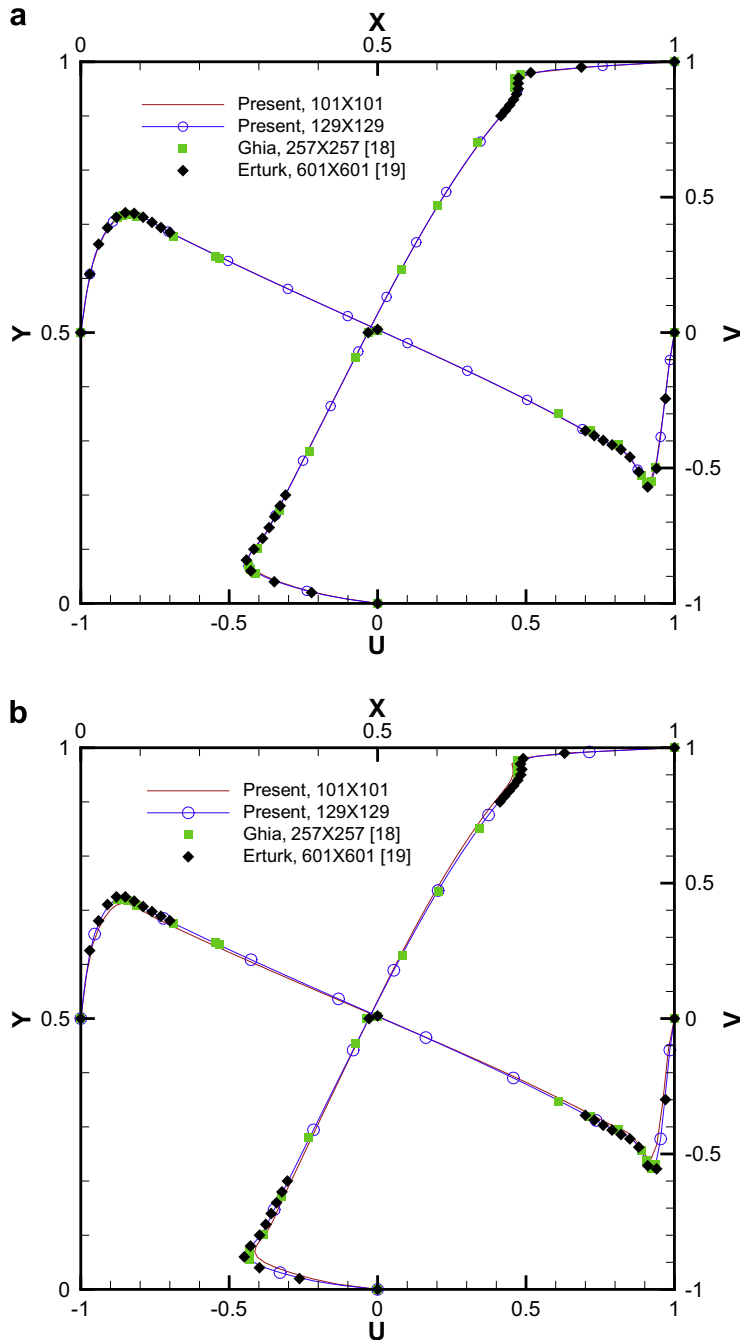

Fig. 13. Comparison of the predicted mid-plane velocity profiles $u(x, 0.5)$ and $v(0.5, y)$ with the benchmark solutions obtained at $Re = 5000$ and 7500. (a) $Re = 5000$ and (b) $Re = 7500$.

Table 7

Comparison of the predicted eddy centers (primary eddy P, corner eddies BL and BR, and the eddy T near the cavity roof) with Ghia et al. [18] and Erturk et al. [19] for the cases investigated at $Re = 5000$ and 7500 using the present scheme.

Symbol	Authors	Re	
		5000	7500
Primary	Present	0.5149, 0.5359	0.5127, 0.5327
	[18]	0.5117, 0.5352	0.5117, 0.5322
	[19]	0.5150, 0.5350	0.5133, 0.5317
T	Present	0.0644, 0.9091	0.0667, 0.9114
	[18]	0.0625, 0.9102	0.0664, 0.9141
	[19]	0.0633, 0.9100	0.0667, 0.9133
BL1	Present	0.0727, 0.1372	0.0638, 0.1537
	[18]	0.0703, 0.1367	0.0645, 0.1504
	[19]	0.0733, 0.1367	0.0650, 0.1517
BR1	Present	0.8000, 0.0725	0.7820, 0.0646
	[18]	0.8086, 0.0742	0.7813, 0.0625
	[19]	0.8050, 0.0733	0.7900, 0.0650
BL2	Present	0.0076, 0.0079	0.0131, 0.0106
	[18]	0.0117, 0.0078	0.0117, 0.0117
	[19]	0.0083, 0.0083	0.0117, 0.0117
BR2	Present	0.9740, 0.0207	0.9439, 0.0513
	[18]	0.9805, 0.0195	0.9492, 0.0430
	[19]	0.9783, 0.0183	0.9517, 0.0417
Mesh points	Present	128	128
	[18]	257	257
	[19]	601	601

In the above, $\underline{x}$ denotes the distance vector to the interface. δ is the regularized function, which is set at $\delta = 1.1\Delta x$ in the present study. This problem has been regarded as a fairly tough test for assessing the pure advection scheme applied to solve the problem containing a sharp solution gradient.

The third-order accurate Runge–Kutta solutions, predicted at 201×201 grid size, after five revolutions for the case with $k = 0$ were compared and shown in Fig. 10. For the sake of completeness, the 3D contours are also plotted at different revolutions in Fig. 11. Good agreement with the exact (or initial) solution schematic in the same figure is clearly seen.

6.4. Lid-driven cavity flow problem

With the success of predicting the solutions in smooth region and the non-oscillating solutions in regions of interior layer from the scalar convection–diffusion scalar equation, we will apply the dual-compact scheme to simulate the high Reynolds number Navier–Stokes flow in a cavity with an upper lid schematic in Fig. 12. In a square with 101×101 and 129×129 nodal points, the predicted velocity profiles $u(0.5, y)$ and $v(x, 0.5)$ at $Re = 5000$ and 7500 will be compared with the steady-state benchmark solutions of Ghia [18] and Erturk [19]. Good agreement between the simulated and the benchmark mid-sectional velocity profiles is clearly shown in Fig. 13. The predicted eddy centers at T, BL1, BR1, BL2 and BR2, schematic in Fig. 12, are also in good agreement with the benchmark solutions that are summarized in Table 7. The applicability of the proposed scheme to predict the high Reynolds number incompressible flow is therefore confirmed.

7. Concluding remarks

The proposed dual-compact scheme for the approximation of advection and diffusion terms is presented within the three-point stencil framework for the convection–diffusion transport equation. The dispersive and dissipative natures of the proposed scheme have been both rigorously revealed. To verify the proposed scheme, we have considered one problem that is amenable to the exact solution. Also, three benchmark problems featured with interior shear layer and high Reynolds number are investigated for the sake of validation. The computed L_2-error norms and their resulting spatial rates of convergence demonstrate the advantage of employing the proposed scheme to simulate the problems containing possibly the smooth as well as the sharply varying solution profiles.

References

[1] D.B. Spalding, A novel finite difference formulation for differential expressions involving both first and second derivatives, Int. J. Numer. Meth. Eng. 4 (1972) 551–559.

[2] B.P. Leonard, A stable and accurate convective modelling procedure based on quadratic upstream interpolation, Comp. Meth. Appl. Mech. Eng. 19 (1979) 59–98.
[3] C.R. Swaminathan, V.R. Voller, Streamline upwind scheme for control-volume finite elements, part I. Formulations, Numer. Heat Transfer B 22 (1) (1992) 95–107.
[4] G. de Felice, F.M. Denaro, C. Meola, Multidimensional single-step vector upwind schemes for highly convective transport problems, Numer. Heat Transfer B 23 (4) (1993) 425–460.
[5] Yuguo Li, Murray Rudman, Assessment of higher-order upwind schemes incorporating FCT for convection-dominated problems, Numer. Heat Transfer B 27 (1) (1995) 1–21.
[6] Tony W.H. Sheu, S.F. Tsai, Morten M.T. Wang, Monotone multidimensional upwind finite element method for advection–diffusion problems, Numer. Heat Transfer B 29 (3) (1996) 325–344.
[7] Tony W.H. Sheu, S.F. Tsai, S.K. Wang, Monotonic, multidimensional flux discretization scheme for all Peclet numbers, Numer. Heat Transfer B 31 (4) (1997) 441–457.
[8] Christorher K.W. Tam, Jay C. Webb, Dispersion-relation-preserving finite difference schemes for computational acoustics, J. Computat. Phys. 107 (1993) 262–281.
[9] I.A. Abalakin, A.V. Alexandrov, V.G. Bobkov, T.K. Kozubskaya, High accuracy methods and software development in computational aeroacoustics, J. Comput. Meth. Sci. Eng. 2 (3) (2003) 1–14.
[10] F.Q. Hu, M.Y. Hussaini, J.L. Manthey, Low-dissipation and low-dispersion Runge–Kutta schemes for computational acoustics, J. Comput. Phys. 124 (1996) 177–191.
[11] Peter C. Chu, Chenwu Fan, A three-point combined compact difference scheme, J. Comput. Phys. 140 (1998) 370–399.
[12] David W. Zingg, Comparison of high-accuracy finite-difference methods for linear wave propagation, SIAM J. Sci. Comput. 22 (2) (2000) 476–502.
[13] S.K. Lele, Compact finite difference schemes with spectral-like resolution, J. Comput. Phys. 103 (1992) 16–42.
[14] P.H. Chiu, Tony W.H. Sheu, R.K. Lin, An effective explicit pressure gradient scheme implemented in the two-level non-staggered grids for incompressible Navier–Stokes equations, J. Comput. Phys. 227 (2008) 4018–4037.
[15] R.M. Smith, A.G. Hutton, The numerical treatment of convection – a performance comparison of current methods, Int. J. Numer. Meth. Heat Trans. 5 (1982) 439–461.
[16] Jun Zhang, Jennifer J. Zhao, Truncation error and oscillation property of the combined compact difference scheme, Appl. Math. Comput. 161 (1) (2005) 241–251.
[17] S.T. Zalesak, Fully multidimensional flux corrected transport algorithms for fluids, J. Comput. Phys. 48 (1979) 335–362.
[18] U. Ghia, K.N. Ghia, C.T. Shin, High-Re solutions for incompressible flow using the Navier–Stokes equations and a multigrid method, J. Comput. Phys. 48 (1982) 387–411.
[19] E. Erturk, T.C. Corke, C. Gökçöl, Numerical solutions of 2-D steady incompressible driven cavity flow at high Reynolds numbers, Int. J. Numer. Meth. Fluids 48 (2005) 747–774.